Unexpected magnetic coupling oscillations for $L1_0$-MnGa/Co(Fe) films induced by quantum wells

Junwei Tong,[1] Liuxia Ruan,[1] Xiannian Yao,[1] Fubo Tian,[2] Gaowu Qin,[1] and Xianmin Zhang[1,*]

[1]*Key Laboratory for Anisotropy and Texture of Materials (Ministry of Education), School of Material Science and Engineering, Northeastern University, Shenyang 110819, China*

[2]*State key Laboratory of Superhard Materials, College of Physics, Jilin University, Changchun 130012, China*

(Received 12 December 2017; revised manuscript received 23 March 2018; published 24 May 2018)

Exchange magnetic coupling interactions between $L1_0$-MnGa and ultrathin Co (Fe) films were studied by first-principles calculations. An unexpected oscillation of magnetic coupling was observed by varying the thickness of Co or Fe layer. Moreover, the coupling types are different for Co and Fe with $L1_0$-MnGa. The magnetic coupling maintains the ferromagnetic interaction for $L1_0$-MnGa/Fe, even if the thickness of Fe layer varies. Interestingly, a change from ferromagnetic to antiferromagnetic couplings appears alternately for $L1_0$-MnGa/Co till Co thickness is up to 11 atomic layers. The coupling oscillations were attributed to the quantum well states formed in the Co (Fe) films. The orbital characters of the quantum well states were analyzed. Our results are useful to further understand the magnetic coupling interactions and design new magnetic nanostructures.

DOI: 10.1103/PhysRevB.97.184426

I. INTRODUCTION

Exploring quantum effects in magnetic coupling opens an opportunity to manipulate various magnetic properties in magnetic nanostructures. Strongly quantum confined electronic states are being explored to access new two-dimensional geometries for special magnetic applications. Quantum well states (QWS) could result in oscillatory physical properties as a function of two-dimensional material thickness. Such oscillations play a dominant role in changing magnetic material properties, such as magnetocrystalline anisotropy (MCA) energy [1–5], Curie temperature [6], and surface energy [7–9]. The oscillations of MCA energy and orbital magnetic moment for Fe layers on Ag were firstly studied by Li and Dąbrowski with their co-workers [1,3], respectively. These were attributed to the *d*-band QWS in Fe film. It was reported that QWS existed in the nonmagnetic metal layer of a sandwich or superlattice structure, which induce the oscillatory exchange coupling between magnetic films [10–15]. Recently, it was found that the QWS in a magnetic layer could induce the oscillatory exchange coupling through an MgO insulator [16]. As a contrast, direct magnetic couplings among magnetic layers without space layers are especially interesting in both the exploration of magnetic physics and actual device applications by manipulating the coercivitiy and saturation magnetization. Generally, the direct contact of different magnetic layers could result in two types of interface interaction. One is ferromagnetic (FM) interaction and the other one is antiferromagnetic (AFM) exchange coupling. So far, the direct interfacial exchange interaction of magnetic bilayers has been extensively studied, e.g., Ni/Fe and Co/Ni are ferromagnetically coupled and Fe/Gd is antiferromagnetically coupled [17–19]. However, the magnetic coupling oscillation phenomenon of FM layers in direct contact has not been reported. This investigation should be valuable for the fundamental science and potential applications in spintronics.

Recently, $L1_0$-MnGa film, a new spintronics material, has attracted huge attention for potential applications in magnetoresistive random access memories (MRAM) [20–26] because of its large perpendicular magnetic anisotropy energy of 26 Merg/cm^3 [27] and an ultralow low Gilbert damping constant of 0.0003 [28]. Moreover, the material also shows other interesting applications. $L1_0$-MnGa film shows an ultrahigh coercivity prepared by a molecular beam epitaxy, which is potentially used in perpendicular magnetic recording bits and oscillator pillars [29]. The Hall effect was also explored in $L1_0$-MnGa films [30,31]. Co and Fe are most popular FM materials studied in both basic science and electronic industry. In spintronics, they have been used as insert layers to improve the interface quality in magnetoresistance (MR) devices. Ma *et al.* reported that $L1_0$-MnGa/Co/MgO/CoFeB junctions show a significant enhancement of MR ratio by Co layer insertion [20]. Kubota *et al.* found that the MR ratios for $L1_0$-MnGa/Fe/MgO/CoFe could be enhanced over one order of magnitude after Fe insertion [32]. Although lots of experimental studies were performed to understand the magnetic couplings of $L1_0$ - MnGa/Co(Fe) and their correlation with MR enhancements [33–35], a theoretical understanding of the interface interactions in both MnGa/Co and MnGa/Fe bilayers is still lacking [36].

In this paper, we studied the direct exchange coupling interaction between $L1_0$-MnGa and Co (Fe) films by first-principles calculations. An unexpected oscillation of magnetic coupling was observed by varying the thickness of ultrathin Co or Fe layer. There is no spacer layer in the present study, unlike previous investigations [10–16]. Moreover, the coupling types are different for Co and Fe with $L1_0$-MnGa. The magnetic coupling maintains the FM interaction for $L1_0$-MnGa/Fe, even if the thickness of Fe layer varies. Interestingly, a change from FM to AFM coupling appears alternately for $L1_0$-MnGa/Co till Co thickness is up to 11 atomic layers. It is found that

*Corresponding author: zhangxm@atm.neu.edu.cn

the coupling oscillations originate from the QWS in Co or Fe ultrathin film confined by the vacuum level and the energy gap of $L1_0$-MnGa substrate.

II. COMPUTATIONAL DETAILS

The first-principles calculations based on density functional theory (DFT) are performed using the Vienna *ab initio* simulation package (VASP) code [37,38]. The Perdew-Burke-Ernzerhof of spin-polarized generalized gradient approximation (PBE-GGA) [39] is applied for the exchange and correlation functional. The energy cutoff of the plane-wave basis is set as 500 eV and the Monkhorst-Pack k-point Brillouin sampling is used. The k-point grid contained $21 \times 21 \times 1$ points for all slabs and $21 \times 21 \times 21$ points for all bulk materials along a, b, and c directions, respectively. The vacuum separating two periodically repeated slabs along a direction perpendicular to the surface of the slabs was chosen to be 15 Å long. Geometry optimization was performed until the forces acting on atoms were less than 0.01eV/Å. More details about the computational procedure and models can be found in Ref. [40].

This study is organized as follows. First, the surface formation energy and interface energy of $L1_0$-MnGa (001) with different terminals (Mn or Ga) is calculated. Second, the difference of the total energy between FM and AFM states as a function of the number of Co (Fe) layers is calculated. Unexpected results for the magnetic coupling oscillation between the above materials are observed. Third, calculations of the band structures and the wave functions are further performed to analyze the oscillation mechanism. Finally, QWS are proposed as the physical origin of the oscillation phenomenon.

III. RESULTS AND DISCUSSION

A. Surface and interface calculations

The fct-like unit cell of $L1_0$-MnGa is shown in Fig. 1(a). The optimized lattice parameters are $a = 3.84$ Å and $c = 3.64$ Å, agreeing well with the reports in literature [27,28,41,42]. These lattice parameters were used for our calculations in this study. The smaller bct-like unit cell [Fig. 1(b)] is utilized, as it allows lower computational cost due to a smaller basis [43]. $L1_0$-MnGa is a perpendicular magnetic anisotropy material and the easy magnetization axis of $L1_0$-MnGa is [001] [21], as shown in Fig. 1(c). Therefore the (001) surface of $L1_0$-MnGa is used to perform the calculations. To investigate the thermodynamic stability of the interface of $L1_0$-MnGa/Co(Fe) bilayers, firstly, the surface formation energy of $L1_0$-MnGa (001), $\gamma_{L1_0\text{-MnGa}}$, is calculated by the equation [44,45]

$$\gamma_{L1_0\text{-MnGa}} = \frac{1}{2A}\Big[E_{\text{slab}}(n_{\text{Mn}},n_{\text{Ga}}) - \frac{1}{2}(n_{\text{Mn}}+n_{\text{Ga}}) \times \mu_{L1_0\text{-MnGa(bulk)}} - \frac{1}{2}(n_{\text{Mn}}-n_{\text{Ga}})\Delta\mu\Big], \quad (1)$$

where A is the corresponding surface area, E_{slab} is the total energy of the system under study, and n_{Mn} and n_{Ga} are the corresponding numbers of atoms in the system. The chemical potential of $L1_0$-MnGa is defined as $\mu_{L1_{0\text{-MnGa}}(\text{bulk})} = \mu_{\text{Mn}} + \mu_{\text{Ga}}$ and $\Delta\mu$ is defined as $\Delta\mu = \mu_{\text{Mn}} - \mu_{\text{Ga}}$. Here, μ_{Mn} and μ_{Ga} are the chemical potentials for Mn and Ga, respectively.

In addition, $\mu_{\text{Mn}} < \mu_{\text{Mn(bulk)}}$ and $\mu_{\text{Ga}} < \mu_{\text{Ga(bulk)}}$, otherwise bulk Mn or Ga would form, in which $\mu_{\text{Mn(bulk)}}$ means the Mn chemical potential in Mn bulk (for the $\mu_{\text{Mn(bulk)}}$ calculation, we chose the $\gamma-$Mn phase with its simple antiferromagnetic structure [46,47]) and $\mu_{\text{Ga(bulk)}}$ means the Ga chemical potential in Ga bulk. Then, the limits to plot $\Delta\mu$ are defined by $\mu_{\text{Mn(bulk)}} - \mu_{\text{Ga(bulk)}} - E_f < \Delta\mu < \mu_{\text{Mn(bulk)}} - \mu_{\text{Ga(bulk)}} + E_f$, where $E_f = \mu_{\text{Mn(bulk)}} + \mu_{\text{Ga(bulk)}} - \mu_{L1_0\text{-MnGa}}$ is the heat of formation of bulk $L1_0$-MnGa from bulk Ga and bulk Mn. The surface formation energies for Mn and Ga terminated $L1_0$-MnGa(001) surfaces as a function of $\Delta\mu$, are presented in Fig. 2(a). Note that the surface formation energy for the Ga-terminated surface is much lower than that for the Mn-terminated surface over the entire $\Delta\mu$ chemical potential. In equilibrium conditions, the surface of $L1_0$-MnGa(001) is Ga-terminated.

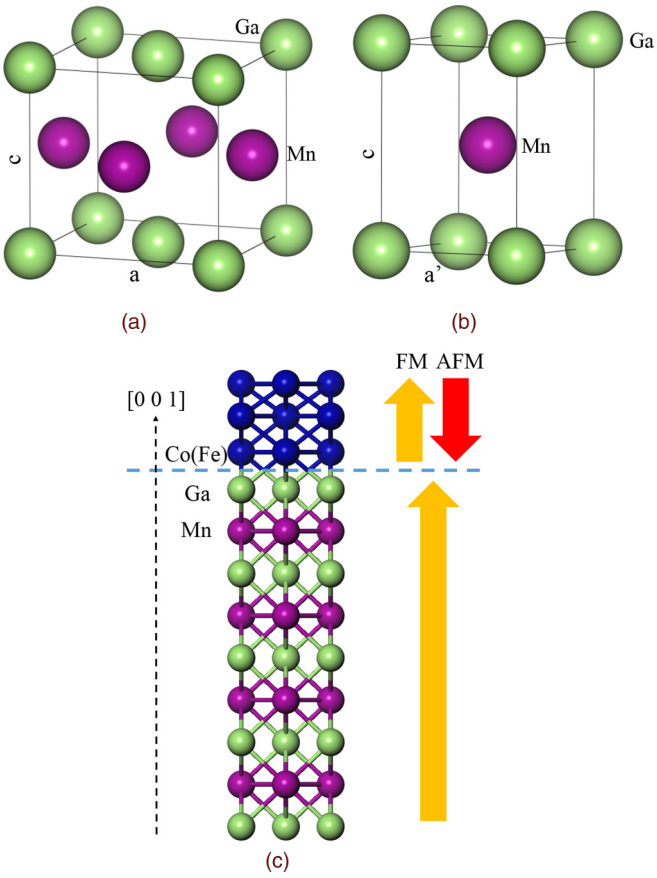

FIG. 1. Schematic illustration of $L1_0$-MnGa tetragonal crystal structure and $L1_0$-MnGa/Co(Fe) bilayer model. (a) The fct-like unit cell, (b) bct-like unit cell. $a = \sqrt{2}a'$. (c) $L1_0$-MnGa/Co(Fe) slab for three atomic layers of Co(Fe) on $L1_0$-MnGa with Ga termination. Initial magnetic configurations are represented by yellow and red arrows, which are parallel and antiparallel to the magnetization direction of the bottom $L1_0$-MnGa layers, respectively. The initial magnetic states are only considered for the Mn, Co, and Fe atoms.

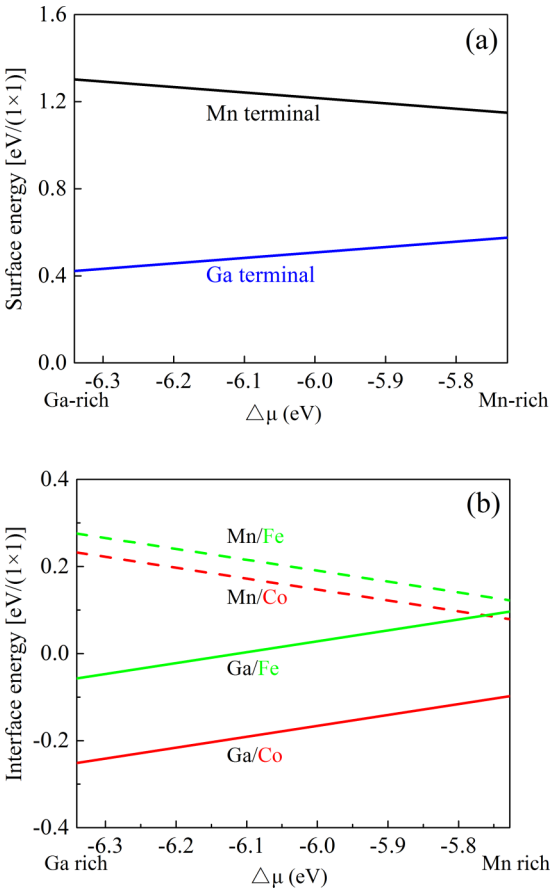

FIG. 2. Surface formation energy of $L1_0$-MnGa film and interface energy of $L1_0$-MnGa/Co(Fe) bilayer. (a). Surface formation energy plots [for Ga and Mn termination as a function of $\Delta\mu(\Delta\mu = \mu_{\mathrm{Mn}} - \mu_{\mathrm{Ga}})$]. (b) Interface energy plots [in eV/(1 × 1)] of Ga/Co(Fe) and Mn/Co(Fe) as a function of $\Delta\mu$.

Secondly, the interface energy of $L1_0$-MnGa/Co(Fe), $\gamma_{L1_0\text{-MnGa/Co(Fe)}}$, is calculated by the equation [48–50]

$$\gamma_{L1_0\text{-MnGa/Co(Fe)}} = \frac{1}{A_i}(E_{L1_0\text{-MnGa/Co(Fe)}} - E_{L1_0\text{-MnGa}} - E_{\mathrm{Co(Fe)}}) + \gamma_{L1_0\text{-MnGa}} + \gamma_{\mathrm{Co(Fe)}}, \quad (2)$$

where A_i is the corresponding interface area, $E_{L1_0\text{-MnGa/Co(Fe)}}$, $E_{L1_0\text{-MnGa}}$, and $E_{\mathrm{Co(Fe)}}$ are the total energies of the $L1_0$-MnGa/Co(Fe) bilayers, $L1_0$-MnGa slabs, and Co(Fe) slabs embedded in vacuum, respectively. $\gamma_{L1_0\text{-MnGa}}$ is the surface energy of $L1_0$-MnGa with Ga terminal or Mn terminal for Ga/Co(Fe) or Mn/Co(Fe) interface, respectively. $\gamma_{\mathrm{Co(Fe)}}$ is the surface energy of Co(Fe) layer which is defined as: $\gamma_{\mathrm{Co(Fe)}} = \frac{1}{2A_s}(E_{\mathrm{Co(Fe)}} - n_{\mathrm{Co(Fe)}}\mu_{\mathrm{Co(Fe)}})$, where A_s is the corresponding surface area, $n_{\mathrm{Co(Fe)}}$ are the corresponding numbers of atoms in the Co(Fe) slabs and $\mu_{\mathrm{Co(Fe)}}$ means the Co(Fe) chemical potential in Co(Fe) bulk. The calculated results are plotted as function of $\Delta\mu$ in Fig. 2(b). Lower interface energy means a more stable interface. As a result, Ga/Co(Fe) is the interface of $L1_0$-MnGa and Co(Fe) layers in equilibrium conditions.

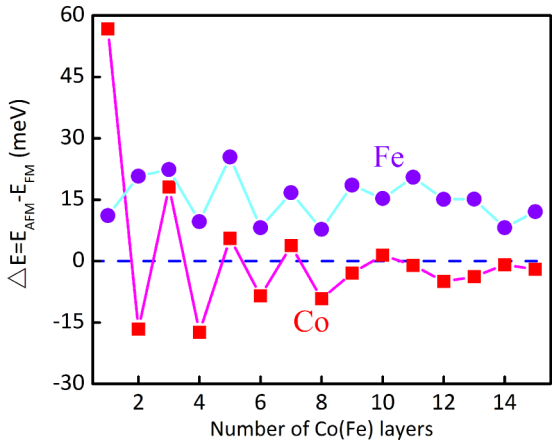

FIG. 3. Total energy difference between FM and AFM states as a function of the number of Co(Fe) layers. $L1_0$-MnGa/Co (red squares) and $L1_0$-MnGa/Fe (purple circles).

B. Magnetic coupling calculation

To explore magnetic coupling between $L1_0$-MnGa and Co (Fe) film, the total energy for AFM and FM magnetic states $L1_0$-MnGa/Co(Fe) with ultrathin Co (Fe) films by varying their thickness are calculated. Figure 1(c) shows the model that we adopted to calculate the magnetic coupling. AFM and FM mean that Co and Fe layers coupled with $L1_0$-MnGa layer by AFM and FM, respectively.

The difference of total energy between AFM and FM magnetic states of $L1_0$-MnGa/Co(Fe) is denoted as $\Delta E = E_{\mathrm{AFM}} - E_{\mathrm{FM}}$, where E_{AFM} is the energy of AFM state $L1_0$-MnGa/Co(Fe) and $\mathrm{E_{FM}}$ is the energy of FM state $L1_0$-MnGa/Co(Fe). The calculated results are shown in Fig. 3. The dash line means there is no energy difference between AFM and FM magnetic sates. The positive and negative values of ΔE correspond to the FM and AFM interactions, respectively. The magnetic coupling for $L1_0$-MnGa layer with a Fe layer is quite different to that with a Co layer. An oscillation of energy difference is observed for different Fe layer thickness. It is found that FM coupling is dominant for $L1_0$-MnGa/Fe, even if the thickness of Fe layers is over 11 atomic layers. This is consistent with the experimental investigation done by Kubota [32,33]. However, for $L1_0$-MnGa/Co bilayer, the AFM and FM interactions appear alternatively with increasing Co layer numbers. When the number of Co layers is even or odd, the magnetic coupling is AFM or FM, respectively. This unexpected oscillation between AFM and FM states with increasing Co layer thickness was shown in Fig. 3. Besides, the coupling in $L1_0$-MnGa/Co remains AFM when the thickness of Co is over 11 atomic layers, agreeing with the previous reports [20,33]. The effect of $L1_0$-MnGa layer numbers on the magnetic coupling is studied in Fig. S1 (see Ref. [40]), indicating the coupling types for $L1_0$-MnGa/Co are independent of the thickness of $L1_0$-MnGa.

C. Band structure analysis

As shown in Fig. 3, it is noted that the magnetic coupling oscillations of $L1_0$-MnGa/Co have a period of 2 monolayers (ML). The period is the same as that previously reported in

MCA energy oscillations of Co films, which originates from the QWS close to $\bar{\Gamma}$ point induced by the confinement of bulk Co spin-down d band with Δ_5 symmetry [51]. The oscillations of MCA for the Co film were also found as a function of Pd thickness and attributed to the QWSs with d symmetry in Pd films [52,53]. Does the present magnetic coupling oscillation of $L1_0$-MnGa/Co also mainly originates from the d band with Δ_5 symmetry? To explore the possible oscillation mechanism, the surface projected bulk bands of both $L1_0$-MnGa and Co (Fe) are plotted in Fig. 4 and Fig. S2 (see Ref. [40]), respectively. One can see that there is a small energy gap around the Fermi energy (E_F) level at $\bar{\Gamma}$ point for the spin-up energy bands of $L1_0$-MnGa, as shown in Fig. 4(a). There exists an energy gap at $\bar{X}$ point in the energy range of -0.7–1 eV for spin-down energy bands of $L1_0$-MnGa, as shown in Fig. 4(b). These energy gaps would limit the extension of electron wave functions into $L1_0$-MnGa film [54]. The surface projected bulk bands of Co are plotted in Figs. 4(c) and 4(d), which show that both spin-up and spin-down electronic states appear at $\bar{\Gamma}$ and $\bar{X}$ points. The energy band of bulk Co along the ΓZ direction was drawn in Fig. 5. The corresponding period of oscillation can be determined by the following formula [3,51], $L = \frac{2\pi}{a}[k_{evn}]^{-1}$, where a is the lattice constant, and k_{evn} is defined as the wave vector spanning the crossing point of the electronic band at the E_F level and the nearest high-symmetry point of the Brillouin zone. The calculated period for a spin-down energy band with Δ_5 symmetry (marked by solid blue circles) is 3.1 ML. This is not consistent with the observed period in Fig. 3. So the oscillation of the magnetic coupling of $L1_0$-MnGa/Co is probably not due to the Co spin-down d band with Δ_5 symmetry. In the previous study, the MCA oscillation period is around 2 ML owing to the Co being an fcc structure [51]. We further checked the energy band of Co along the ΓX direction with fcc structure, as shown in Fig. S3 (see Ref. [40]). It is found that the period determined by the spin-down energy band with Δ_5 symmetry is 2.1 ML, agreeing with the literature [51]. Nerveless, for the present $L1_0$-MnGa/Co investigation, the in-plane lattice parameter of Co is fixed to match the $L1_0$-MnGa lattice parameter, resulting in the Co bct structure and the period being 3.1 ML. The optimized lattice parameter of bct Co is $c = 3.02$ Å. The energies for QWS originating from the spin-down band of bulk Co with Δ_5 symmetry at the $\bar{\Gamma}$ point for AFM $L1_0$-MnGa/Co and FM $L1_0$-MnGa/Co are shown in Figs. 6(a) and 6(b). It is found that the period of the QWS is almost 3 ML and agrees with the energy band analysis in Fig. 5. Whenever a QWS crosses the Fermi energy level, it adds energy to the system [11]. In Figs. 6(a) and 6(b), it is noted that the crossing points of QWS energy and E_F level appear for the Co layer numbers at about 4, 7, and 10, which are completely different with the coupling change with increasing Co layer thickness (see Fig. 3). Moreover, the crossing points are the same for both AFM and FM states. Thus the magnetic coupling oscillation for $L1_0$-MnGa/Co does not originate from the spin-down band of bulk Co with Δ_5 symmetry near the $\bar{\Gamma}$ point.

In Fig. 5, the calculated period of the band marked by open blue circles is 2.1 ML, which corresponds to the spin-down energy band with $\Delta_{2'}$ symmetry [3]. A possible relation with the present $L1_0$-MnGa/Co coupling oscillation should be clarified. So the energies for QWS from the spin-down band

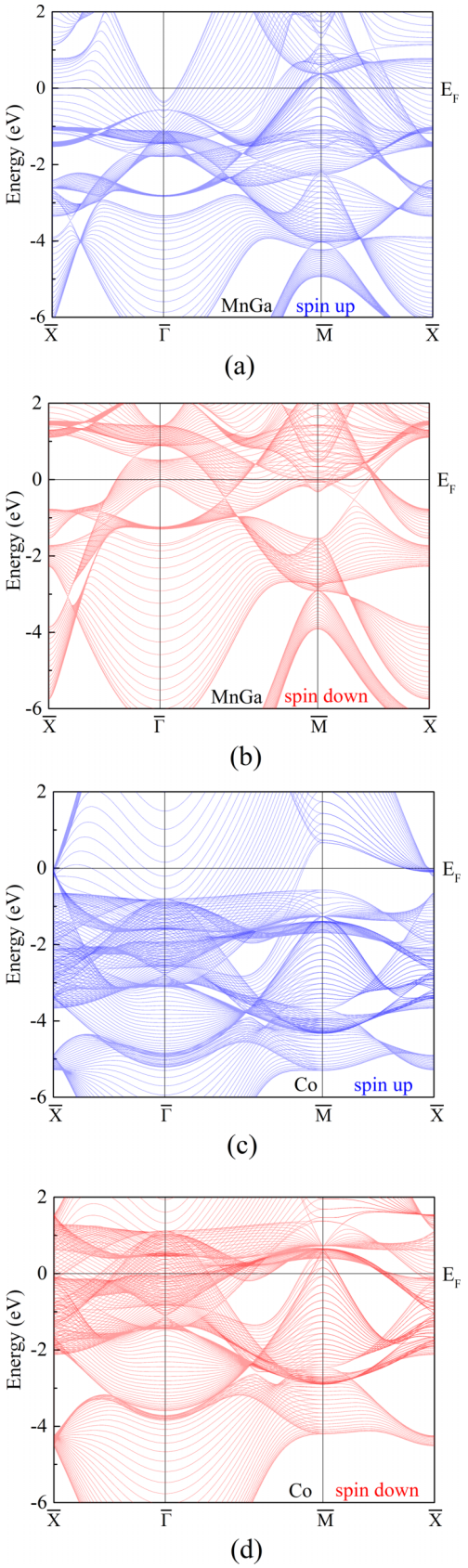

FIG. 4. Band structures of bulk $L1_0$-MnGa [(a) and (b)] and bulk Co [(c) and (d)]. The states for both $L1_0$-MnGa and Co were projected onto the (001) surface Brillouin zone. Blue color for spin-up bands [(a) and (c)] and red color for spin-down bands [(b) and (d)].

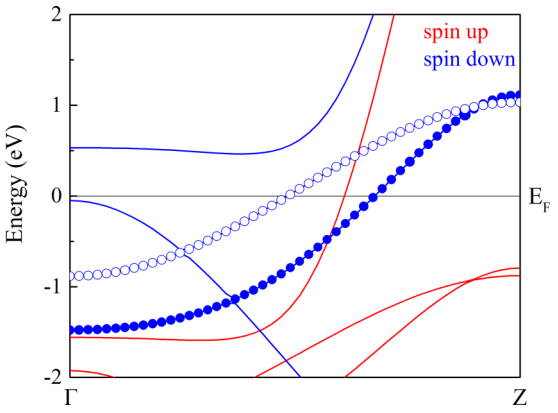

FIG. 5. Spin-resolved band structure of bct Co. The curves with red (blue) color are the spin-up (down) spin-split bands. The band marked by solid blue circles is the spin-down Δ_5 band. The band marked by open blue circles is the spin-down $\Delta_{2'}$ band.

of bulk Co with $\Delta_{2'}$ symmetry for both AFM $L1_0$-MnGa/Co and FM $L1_0$-MnGa/Co at the $\bar{\Gamma}$ point are plotted, as shown in Figs. 6(c) and 6(d). Even though the period of the QWS as a function of Co layer thickness is 2 ML, there is no energy difference between AFM and FM magnetic sates and the crossing points are same for both AFM and FM states. Thus the QWS in the spin-down energy band with $\Delta_{2'}$ symmetry should also not be the reason for the magnetic coupling oscillation of $L1_0$-MnGa/Co. Based on the above analysis of Figs. 3, 5, and 6, we could definitely conclude that the Co d bands near the $\bar{\Gamma}$ point are not responsible for the observed oscillation in Fig. 3. The energy band of bulk Fe and the energies for QWS from the spin-down band of bulk Fe with Δ_5 symmetry for $L1_0$-MnGa/Fe at the $\bar{\Gamma}$ point are shown in Figs. S4 and S5 (see Ref. [40]). It could be concluded that the magnetic coupling oscillation for $L1_0$-MnGa/Fe does not originate from the d band near the $\bar{\Gamma}$ point.

The cross section of the Fermi surface for bulk Co(001) was shown in Fig. 7. One could find the relation between the period of QWS and the corresponding energy band [11,51,55]. The period of extremal A at Γ point is about 3 ML, which is from the d band with Δ_5 symmetry [51]. There are two extreme value points corresponding to around 2-ML period, as labeled by B and C, respectively. B is from the spin-down d band with $\Delta_{2'}$ symmetry. The above analysis based on Figs. 5 and 6 have demonstrated that both A and B are not the reason for the observed coupling oscillation in Fig. 3. The extremal C is close to the X point, which should be responsible for the magnetic coupling oscillation for $L1_0$-MnGa/Co. The cross section of the Fermi surface for bulk Fe(001) is shown in Fig. S6 (see Ref. [40]). There also exist an extremum near X point for the spin-up band, which induces a period of QWS of 2 ML.

The spin-down energy band structures for the AFM coupling $L1_0$-MnGa/Co(n) with Co of 1–6 layers (n means the number of Co layer) are plotted in Fig. 8. The weights of the Co atoms are projected onto the band dispersions and marked by green circles. It is found that there are some bands at $\bar{X}$

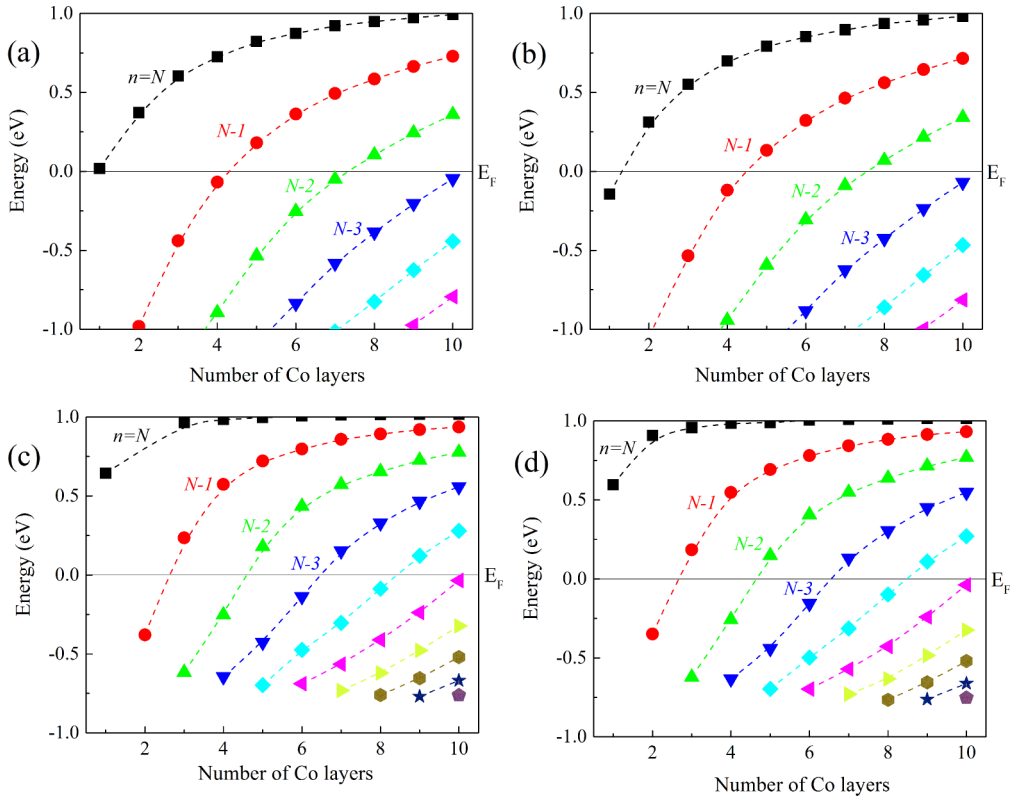

FIG. 6. Energies of QWS in Co layers vs Co thickness. (a) and (b) are from the spin-down Δ_5 band of bulk Co. (c) and (d) are from the spin-down $\Delta_{2'}$ band of bulk Co. (a) and (c) correspond to AFM $L1_0$-MnGa/Co spin-up band at the $\bar{\Gamma}$ point. (b) and (d) are correspond to FM $L1_0$-MnGa/Co spin-down band at the point. The energies of QWS with quantum number $n = N–l$, where N is the number of Co layers, l is an integer, are joined by dotted lines.

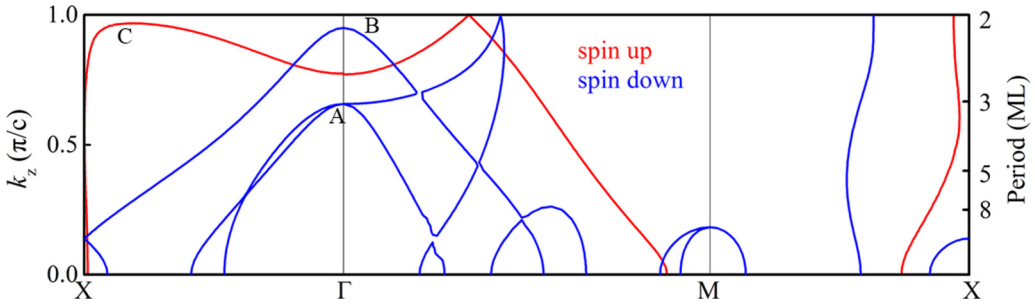

FIG. 7. Cross section of the Fermi surface for bulk Co (001). The red (blue) lines mean the cross section of the Fermi surface for spin-up (down) energy band.

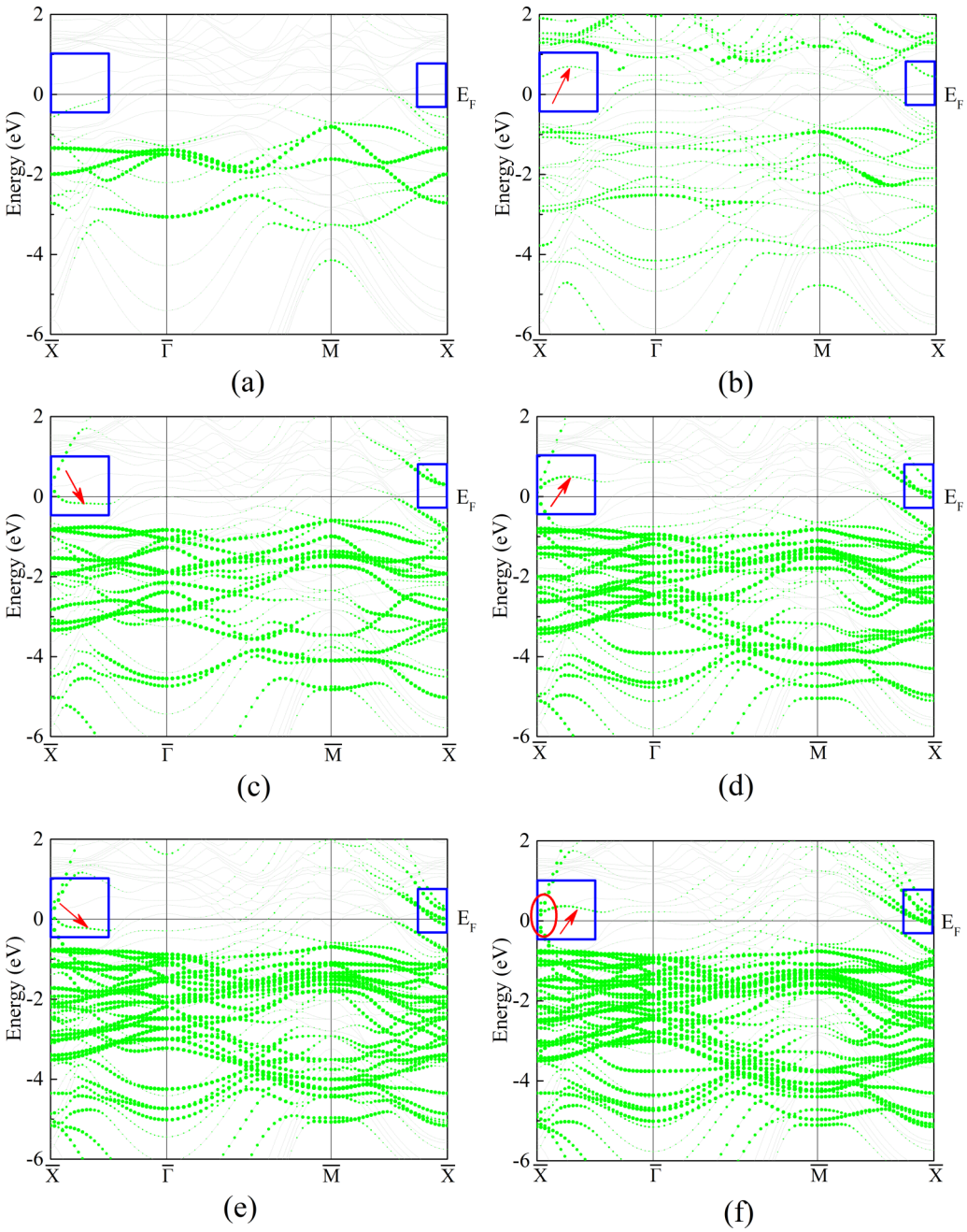

FIG. 8. Spin-down energy bands for AFM coupling in $L1_0$-MnGa/Co with different layer numbers of Co. (a) 1, (b) 2, (c) 3, (d) 4, (e) 5, and (f) 6 layers. The weights of the Co atoms are projected onto the band dispersions and marked by green circles.

point in the energy range of −0.7–1 eV and merge into bulk states along the $\bar{X} \rightarrow \bar{\Gamma}$ and $\bar{X} \rightarrow \bar{M}$ directions, as labeled by blue rectangles in Figs. 8(a)–8(f). The number of those bands increases with increasing Co layer numbers. Moreover, compared with Figs. 8 and 4(b), the location of those bands is just within the energy gap of bulk $L1_0$-MnGa. A common band with gray color appeared above the E_F in the energy gap for all the samples, as shown in Fig. 8. This band is the surface band of $L1_0$-MnGa. The other bands weighted by green circles originate from the QWS, which are located within the Co layer. This will be described in detail as follows.

The spin-up energy bands for FM coupling $L1_0$-MnGa/Co could be found in Fig. S7 (see Ref. [40]). It is noted that the position at $\bar{X}$ point in the energy range of −0.7–1 eV is not the energy gap of $L1_0$-MnGa and it corresponds to the spin-up energy band of $L1_0$-MnGa, as shown in Fig. 4(a). Compare the result of Fig. 8 with that of Fig. S7 (see Ref. [40]), the energy band difference marked by green circles in the blue rectangle between AFM and FM state in $L1_0$-MnGa/Co is clearly observed. It is noted that a special band (denoted by a red arrow) appears in the AFM states but does not appear in the FM states. Particularly, the location of this band strongly depends on the Co layer thickness. When the number of upper Co layers is odd, the band is lower than E_F [see Figs. 8(c) and 8(e)]. When the number of upper Co layers is even, the band is higher than E_F [see Figs. 8(b), 8(d), and 8(f)]. As a result, the energy of AFM coupling in $L1_0$-MnGa/Co increases when the number of Co layers is odd. Correspondingly, the magnetic coupling strength (ΔE) becomes larger when the number of Co layers is odd. Therefore an oscillation of the coupling strength could be expected with increasing Co layer thickness, as shown in Fig. 3. This could be further demonstrated from the viewpoint of the density of states (DOS). The band of $L1_0$-MnGa shows a broad distribution of the DOS across E_F as shown in Fig. S8(a) (see Ref. [40]). The coupling between 3*d* metals mainly depends on the Coulomb repulsion and Pauli exclusion, which rely on the band structure and occupancy. So the Pauli exclusion effect dominates the coupling interactions for $L1_0$-MnGa/Co bilayers [20,56], suggesting electrons near E_F are antiparallelly spin-coupled. The DOS of both bulk Co and Fe are shown in Figs. S8(b) and S8(c) (see Ref. [40]). It is shown that the spin polarization of Co is negative while Fe is positive. Thus the different spin polarizations make the magnetic coupling for thick Co and Fe layers in $L1_0$-MnGa AFM and FM, respectively [20]. The bands (denoted by red arrows) in Fig. 8 increase the DOS of spin-up energy bands near E_F, which reduces the AFM coupling strength between Co (Fe) and $L1_0$-MnGa. Therefore the magnetic coupling is oscillatory.

To understand the bands within the energy gap (blue rectangles), the in-plane average electron charge densities and partial charge density [57] are plotted (Fig. 9) for the bands at $\bar{X}$ point corresponding to the 6 atomic Co layers on $L1_0$-MnGa [the bands are labeled by a red circle in Fig. 8(f)]. The states were drawn in order of energy from low (a) to high (f). The dash lines with green, purple, and blue color indicate the position of Ga, Mn, and Co atoms, respectively. It is observed that the charge density (red line) is only located in the Co layers, without any extension into the $L1_0$-MnGa substrate, as shown in Figs. 9(a)–9(d) and 9(f). So those states are from

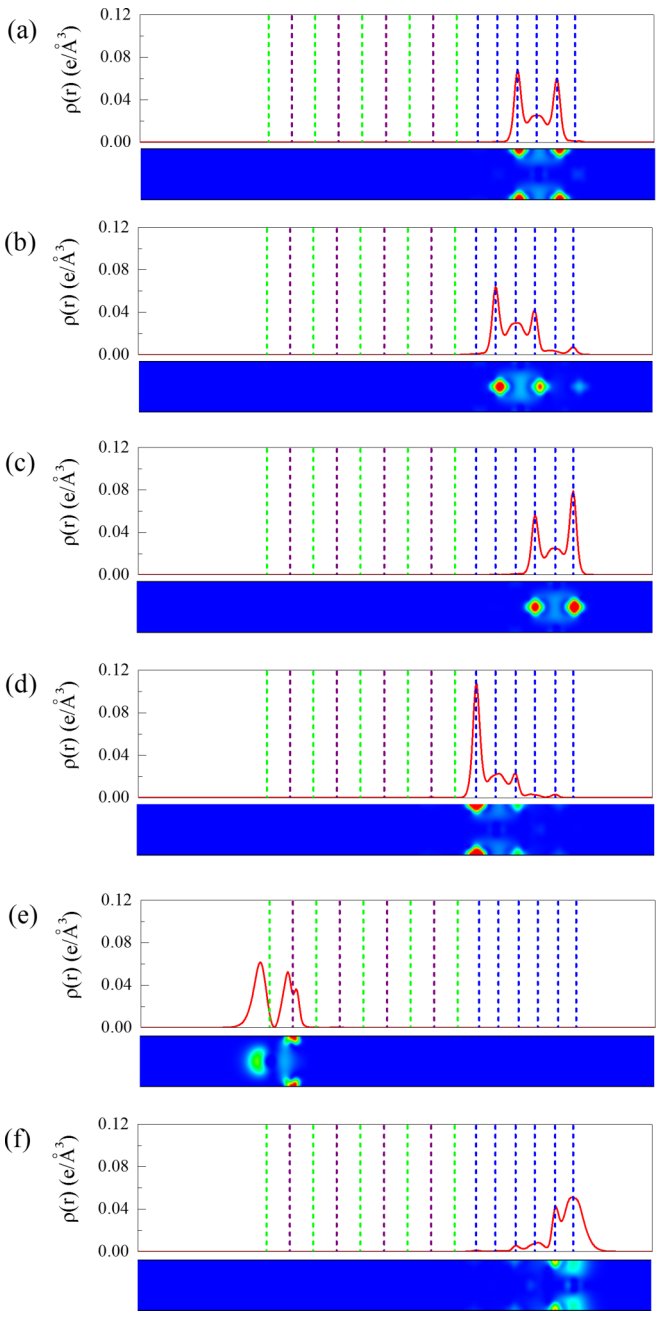

FIG. 9. The in-plane average electron charge densities (up) and partial charge density of (110) surface (down) at the $\bar{X}$ point, which corresponds to the six atomic Co layers on $L1_0$-MnGa [the bands are labeled by a red circle in Fig. 8(f)]. The states were drawn in order of energy from low (a) to high (f). The color scale is from 0.00 (blue) to 0.04 (red) electrons per Å^3. The green, purple, and blue shot dash lines indicate the position of Ga, Mn, and Co atoms, respectively.

the QWS confined in the Co film, which correspond to the bands weighted by green circles in Figs. 8(f). In Fig. 9(e), it is found that the charge density is located in the surface of the $L1_0$-MnGa layer, indicating the common band with gray color in Fig. 8 is the surface band of the $L1_0$-MnGa layer. The band structures and the in-plane average electron charge densities for $L1_0$-MnGa/Fe are also shown in Figs. S9–S11 (see Ref. [40]). The results are similar with these of $L1_0$-MnGa/Co.

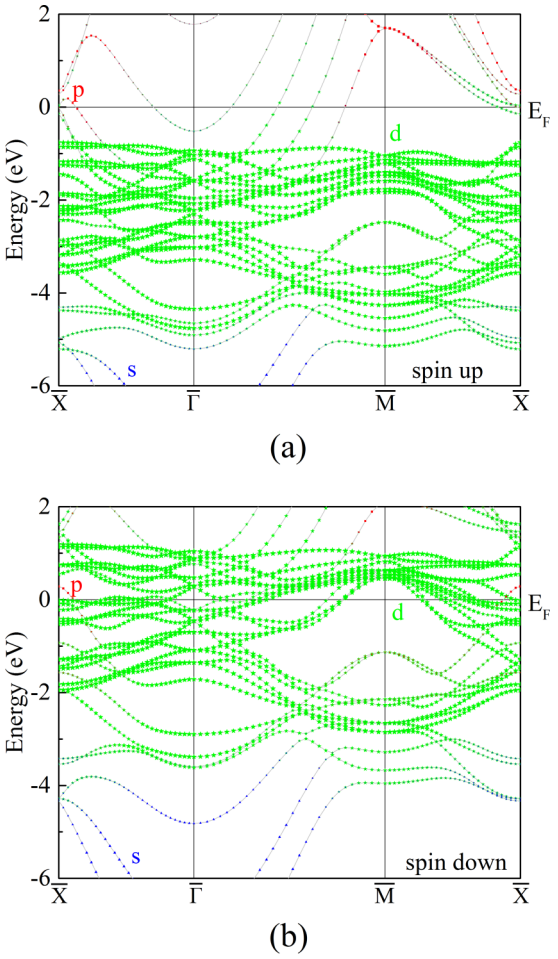

FIG. 10. Band structure of five atomic layers of free-standing Co(001) films for spin-up states (a) and spin-down states (b). The weights of the s, p, and d orbitals are projected onto the band dispersions, marked by blue triangles, red squares, and green stars, respectively.

In the following, we will further discuss the physical origin of the bands as labeled by blue rectangles in Fig. 8. The spin-up and spin-down band structures with five atomic layers of free-standing Co(001) films as a representative example are shown in Fig. 10. The s, p, and d orbital characters are donated by blue triangles, red squares, and green stars, respectively. The flat bands of d electrons show they are more localized than these s and p electrons. The spin-up (down) energy bands of AFM state $L1_0$-MnGa/Co is composed by the spin-up (down) energy bands of $L1_0$-MnGa and spin-down (up) energy bands of Co. The spin-up (down) energy bands of FM state $L1_0$-MnGa/Co is composed by the spin-up (down) energy bands of $L1_0$-MnGa and spin-up (down) energy bands of Co. When the $L1_0$-MnGa layer and Co layer are antiferromagnetically coupled [see Figs. 10(a) and 4(b)], the p electrons and a small amount of s and d character of Co layer is locate in the energy gap of $L1_0$-MnGa. When the $L1_0$-MnGa layer and Co layer are ferromagnetically coupled [see Figs. 10(b) and 4(b)], the flat d bands and one p band of Co layer are located in the energy gap of $L1_0$-MnGa. Thus the vacuum level on the top of the Co layer and the band gap of $L1_0$-MnGa acting as barriers form a quantum well. So the QWS of $L1_0$-MnGa/Co (Fig. 8) originate mostly from the p electrons of the Co layer.

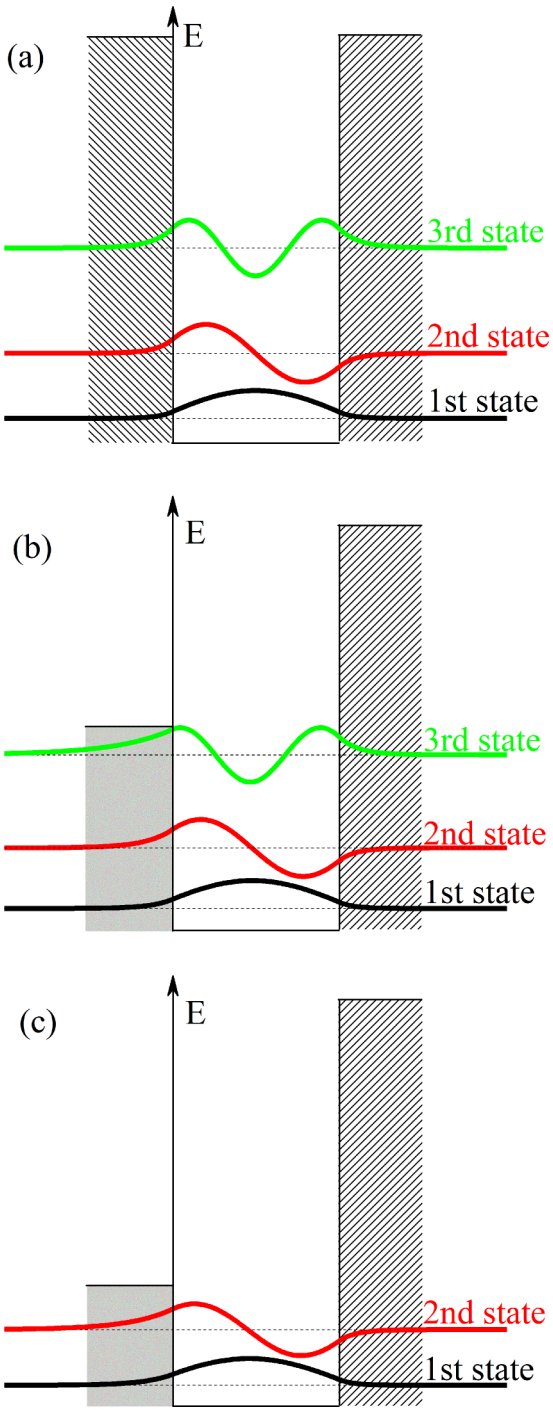

FIG. 11. One-dimensional finite square potential well models. (a) The height of the potentials is 5 eV for both barriers. (b) The height of the potentials is 2.5 eV for the left barrier and 5 eV for the right barriers. (c) The height of the potentials is 1.5 eV for the left barrier and 5 eV for the right barriers. The first three states are shown as the representative occupied states. The width of the well is 1 nm. The mass and charge of the particle are 9.1×10^{-31} kg and 1.6022×10^{-19} C.

In Fig. 10(a), there are five bands for free-standing Co (001) films corresponding to the energy gap position of $L1_0$-MnGa [see Fig. 4(b)]. As a contrast, there are only four bands and three bands for AFM [see Fig. 8(e)] and FM [see Fig. S7(e) in Ref. [40]] $L1_0$-MnGa/Co states corresponding to the energy gap position of $L1_0$-MnGa, respectively. This could be explained by a one-dimensional finite square potential well model [14,54]. In Fig. 11, we use the first three occupied states (first, second, and third states) as representative states to discuss the dependence of QWS on the barrier height. When the electrons are confined with high barriers in both sides, the extension of the wave functions into the barriers is very small, as shown in Fig. 11(a). This result is similar to free Co film embedded in vacuum barriers. If the barrier height in one side reduces, more wave functions obviously extend to the lower barrier. Moreover, the energy of all three bound states (first, second, and third states) in Fig. 11(b) decreases compared to these with high barriers in Fig. 11(a). The barrier height of $L1_0$-MnGa is lower than the vacuum. So this model is similar to the AFM state in $L1_0$-MnGa/Co for the p band located in the energy gap of $L1_0$-MnGa. If the barrier further decreases as shown in Fig. 11(c), the highest bound state (here is a third state) becomes a scattering state [58] and then results in a decrease of number of bands. This is similar to the FM state in $L1_0$-MnGa/Co for the p band located in the conducting band of $L1_0$-MnGa. The band structures of five atomic layers of free-standing Fe(001) films for spin-up states and spin-down states are also shown in Fig. S12 (see Ref. [40]). The coupling mechanism for the $L1_0$-MnGa/Fe film could be also analyzed by the above model.

IV. CONCLUSION

In summary, the steady terminations of $L1_0$-MnGa surface and $L1_0$-MnGa/Co(Fe) interface were studied by *ab initio* calculations. The films with Ga termination show both lower surface formation energy and interface energy than that those with Mn termination. The magnetic states of $L1_0$-MnGa/Co(Fe) bilayers with Ga termination were investigated by varying the thickness of Co(Fe) atomic layers. The coupling interaction of $L1_0$-MnGa/Co film strongly depends on the thickness of the Co layer. The interactions are FM and AFM when the number of Co layers is odd and even, respectively. $L1_0$-MnGa/Fe films maintain FM coupling with varying thickness of Fe layers. The oscillations of the magnetic coupling with increasing numbers of Co(Fe) layers are attributed to QWS in the Co(Fe) layers. This was demonstrated by the systematic band structure calculations of $L1_0$-MnGa, Co, and Fe. The vacuum level on the top of Co or Fe layer and the band gap of $L1_0$-MnGa acting as a barrier form a quantum well. The QWS of $L1_0$-MnGa/Co originate mainly from the p electrons of the Co layer. This could be used to manipulate the magnetic properties of two adjacent magnetic layers for spintronics.

ACKNOWLEDGMENTS

This work was supported by the National Natural Science Foundation of China (Grants No. 51471046 and No. 51525101) and the Fundamental Research Funds for the Central Universities (Grants No. N170205001 and No. N160208001).

[1] J. Li, M. Przybylski, F. Yildiz, X. D. Ma, and Y. Z. Wu, Phys. Rev. Lett. **102**, 207206 (2009).
[2] C.-H. Chang, K.-P. Dou, G.-Y. Guo, and C.-C. Kaun, NPG Asia Mater. **9**, e424 (2017).
[3] M. Dabrowski, T. R. F. Peixoto, M. Pazgan, A. Winkelmann, M. Cinal, T. Nakagawa, Y. Takagi, T. Yokoyama, F. Bisio, U. Bauer, F. Yildiz, M. Przybylski, and J. Kirschner, Phys. Rev. Lett. **113**, 067203 (2014).
[4] F. Gimbert and L. Calmels, Phys. Rev. B **86**, 184407 (2012).
[5] T. R. Dasa, P. Ruiz-Díaz, O. O. Brovko, and V. S. Stepanyuk, Phys. Rev. B **88**, 104409 (2013).
[6] M. Pajda, J. Kudrnovský, I. Turek, V. Drchal, and P. Bruno, Phys. Rev. Lett. **85**, 5424 (2000).
[7] X. Liu and C. Z. Wang, J. Phys.: Condens. Matter **29**, 185504 (2017).
[8] C. M. Wei and M. Y. Chou, Phys. Rev. B **66**, 233408 (2002).
[9] R. K. Kawakami, E. Rotenberg, H. J. Choi, E. J. Escorcia-Aparicio, M. O. Bowen, J. H. Wolfe, E. Arenholz, Z. D. Zhang, N. V. Smith, and Z. Q. Qiu, Nature **398**, 132 (1999).
[10] S. S. P. Parkin, R. Bhadra, and K. P. Roche, Phys. Rev. Lett. **66**, 2152 (1991).
[11] Z. Qiu and N. Smith, J. Phys.: Condens. Matter **14**, R169 (2002).
[12] J. E. Ortega and F. J. Himpsel, Phys. Rev. Lett. **69**, 844 (1992).
[13] Z. Q. Qiu, J. Pearson, A. Berger, and S. D. Bader, Phys. Rev. Lett. **68**, 1398 (1992).
[14] M. D. Stiles, Phys. Rev. B **48**, 7238 (1993).
[15] S. S. P. Parkin, N. More, and K. P. Roche, Phys. Rev. Lett. **64**, 2304 (1990).
[16] S. Wang, K. Xia, T. Min, and Y. Ke, Phys. Rev. B **96**, 024443 (2017).
[17] D. Kim and J. Hong, J. Magn. Magn. Mater. **320**, 528 (2008).
[18] W. L. O'Brien and B. P. Tonner, Phys. Rev. B **52**, 15332 (1995).
[19] Y. Kamiguchi, Y. Hayakawa, and H. Fujimori, Appl. Phys. Lett. **55**, 1918 (1989).
[20] Q. L. Ma, S. Mizukami, T. Kubota, X. M. Zhang, Y. Ando, and T. Miyazaki, Phys. Rev. Lett. **112**, 157202 (2014).
[21] S. Mizukami, A. Sakuma, A. Sugihara, K. Z. Suzuki, and R. Ranjbar, Scripta Mater. **118**, 70 (2016).
[22] J. Winterlik, S. Chadov, A. Gupta, V. Alijani, T. Gasi, K. Filsinger, B. Balke, G. H. Fecher, C. A. Jenkins, F. Casper, J. Kubler, G.-D. Liu, L. Gao, S. S. P. Parkin, and C. Felser, Adv. Mater. **24**, 6283 (2012).
[23] B. Balke, G. H. Fecher, J. Winterlik, and C. Felser, Appl. Phys. Lett. **90**, 152504 (2007).
[24] D. Kim, J. Hong, and L. Vitos, Phys. Rev. B **90**, 144413 (2014).
[25] H. Kurt, K. Rode, M. Venkatesan, P. Stamenov, and J. M. D. Coey, Phys. Rev. B **83**, 020405(R) (2011).
[26] Y. H. Zheng, G. C. Han, H. Lu, and K. L. Teo, J. Appl. Phys. **115**, 043902 (2014).
[27] A. Sakuma, J. Magn. Magn. Mater. **187**, 105 (1998).
[28] S. Mizukami, F. Wu, A. Sakuma, J. Walowski, D. Watanabe, T. Kubota, X. Zhang, H. Naganuma, M. Oogane, Y. Ando, and T. Miyazaki, Phys. Rev. Lett. **106**, 117201 (2011).

[29] L. Zhu, S. Nie, K. Meng, D. Pan, J. Zhao, and H. Zheng, Adv. Mater. **24**, 4547 (2012).
[30] K. K. Meng, J. Miao, X. G. Xu, J. X. Xiao, J. H. Zhao, and Y. Jiang, Phys. Rev. B **93**, 060406 (2016).
[31] F. Wu, E. P. Sajitha, S. Mizukami, D. Watanabe, T. Miyazaki, H. Naganuma, M. Oogane, and Y. Ando, Appl. Phys. Lett. **96**, 042505 (2010).
[32] T. Kubota, Q. Ma, S. Mizukami, X. Zhang, H. Naganuma, M. Oogane, Y. Ando, and T. Miyazaki, Appl. Phys. Express **5**, 043003 (2012).
[33] Q. L. Ma, T. Kubota, S. Mizukami, X. M. Zhang, H. Naganuma, M. Oogane, Y. Ando, and T. Miyazaki, Phys. Rev. B **87**, 184426 (2013).
[34] S. Mizukami, T. Kubota, S. Iihama, R. Ranjbar, Q. Ma, X. Zhang, Y. Ando, and T. Miyazaki, J. Appl. Phys. **115**, 17C119 (2014).
[35] Q. L. Ma, T. Kubota, S. Mizukami, X. M. Zhang, H. Naganuma, M. Oogane, Y. Ando, and T. Miyazaki, Appl. Phys. Lett. **101**, 032402 (2012).
[36] D. Kim and L. Vitos, Sci. Rep. **6**, 19508 (2016).
[37] J. Hafner, J. Comput. Chem. **29**, 2044 (2008).
[38] G. Kresse and J. Furthmüller, Phys. Rev. B **54**, 11169 (1996).
[39] J. P. Perdew, K. Burke, and M. Ernzerhof, Phys. Rev. Lett. **77**, 3865 (1996).
[40] See Supplemental Material at http://link.aps.org/supplemental/10.1103/PhysRevB.97.184426 for more details of computational parameters, models and partial results of $L1_0$-MnGa/Co and $L1_0$-MnGa/Fe for comparison.
[41] H. Niida, T. Hori, H. Onodera, Y. Yamaguchi, and Y. Nakagawa, J. Appl. Phys. **79**, 5946 (1996).
[42] J. Guerrero-Sánchez and N. Takeuchi, Appl. Surf. Sci. **390**, 328 (2016).
[43] A. Edström, J. Chico, A. Jakobsson, A. Bergman, and J. Rusz, Phys. Rev. B **90**, 014402 (2014).
[44] N. Takeuchi and S. E. Ulloa, Phys. Rev. B **65**, 235307 (2002).
[45] N. Takeuchi, Phys. Rev. B **66**, 153405 (2002).
[46] C. Franchini, V. Bayer, R. Podloucky, G. Parteder, S. Surnev, and F. P. Netzer, Phys. Rev. B **73**, 155402 (2006).
[47] J. Hafner and D. Hobbs, Phys. Rev. B **68**, 014408 (2003).
[48] J. Feng, W. Zhang, and W. Jiang, Phys. Rev. B **72**, 115423 (2005).
[49] Y. F. Han, Y. B. Dai, J. Wang, D. Shu, and B. D. Sun, Appl. Surf. Sci. **257**, 7831 (2011).
[50] W. Liu, J. C. Li, W. T. Zheng, and Q. Jiang, Phys. Rev. B **73**, 205421 (2006).
[51] M. Cinal, J. Phys.: Condens. Matter **15**, 29 (2003).
[52] M. Cinal and D. M. Edwards, Phys. Rev. B **57**, 100 (1998).
[53] M. Cinal, J. Phys.: Condens. Matter **13**, 901 (2001).
[54] M. Milun, P. Pervan, and D. P. Woodruff, Rep. Prog. Phys. **65**, 99 (2002).
[55] P. Bruno, Phys. Rev. B **52**, 411 (1995).
[56] J. M. Coey, *Magnetism and Magnetic Materials* (Cambridge University Press, Cambridge, 2010), Chap. 5.
[57] J. M. An, D. Raczkowski, Y. Z. Wu, C. Y. Won, L. W. Wang, A. Canning, M. A. Van Hove, E. Rotenberg, and Z. Q. Qiu, Phys. Rev. B **68**, 045419 (2003).
[58] D. J. Griffiths, *Introduction to Quantum Mechanics* (Cambridge University Press, Cambridge, 2016), Chap. 2.